Supporting Information

Interfacial engineering and chemical reconstruction into $Mo/Mo_2C@CoO@NC$ heterostructure for promoting oxygen evolution reaction

Kai Li,[a,#] Sihui Pan,[a,#] Haiqi Zhang,[a] Qingqing Zhang,[a] Detian Wan,[a] Xiaojun Zeng[a,*]

[a] School of Materials Science and Engineering, Jingdezhen Ceramic University, Jingdezhen 333403, China

* Corresponding author, E-mail: zengxiaojun@jcu.edu.cn (X.J. Zeng)

[#] These authors contributed equally to this work.

OER process

For OER in alkaline electrolyte (pH=14), since OH^- may act as an electron donor, the overall reaction scheme of OER can be expressed as:

$$OH^- + * \rightarrow OH^* + e^- \quad (1)$$

$$OH^* + OH^- \rightarrow O^* + H_2O\ (l) + e^- \quad (2)$$

$$O^* + OH^- \rightarrow OOH^* + e^- \quad (3)$$

$$OOH^* + OH^- \rightarrow O_2\ (g) + H_2O\ (l) + e^- + * \quad (4)$$

where $*$ represents the catalyst and active adsorption site, (l) and (g) represent the liquid and gas phases, and OH*, O*, and OOH* represent the adsorbed intermediates.

TOF calculation

To have better quantification of the activity of $Mo/Mo_2C@CoO@NC$ electrocatalysts, the turnover frequency (TOF) value was calculated from the equation: [1]

$$TOF = (J*A)/(4F*m) \quad (5)$$

where J is the measured current density, A is the surface area of the working electrode, F is the Faraday constant (96485 C mol^{-1}), and m is the number of moles of active materials loaded on the working electrodes. The TOF was calculated by only taking the metal ions (10.51 wt% of cobalt and 43.37 wt% of molybdenum, Table S1) in the catalysts into consideration.

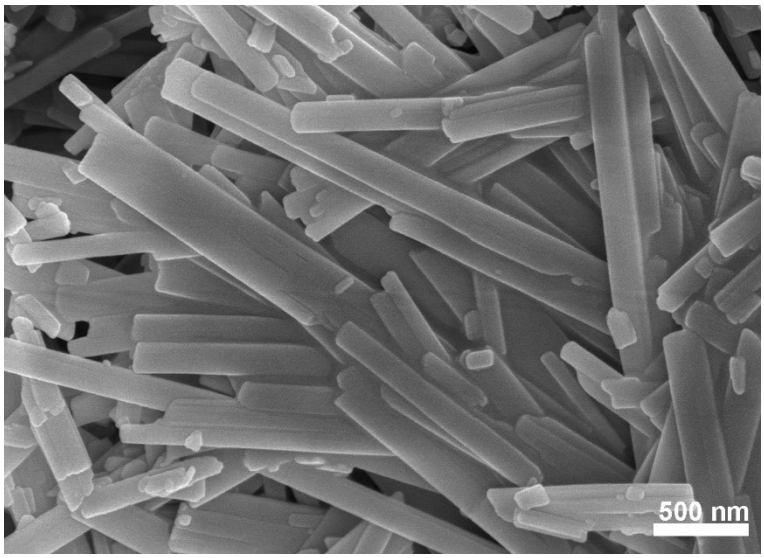

Figure S1. SEM images of MoO_3 nanoribbons.

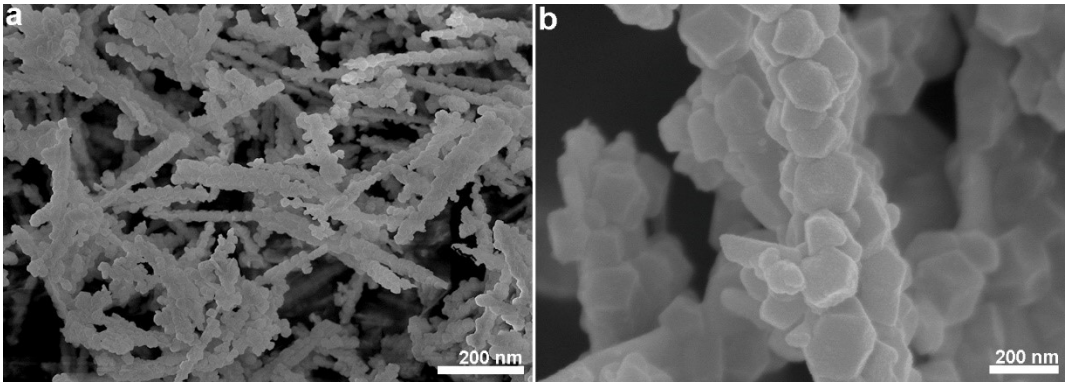

Figure S2. Low-magnification (a) and high-magnification (b) SEM images of MoO_3@ZIF-67 heterogeneous nanoribbons.

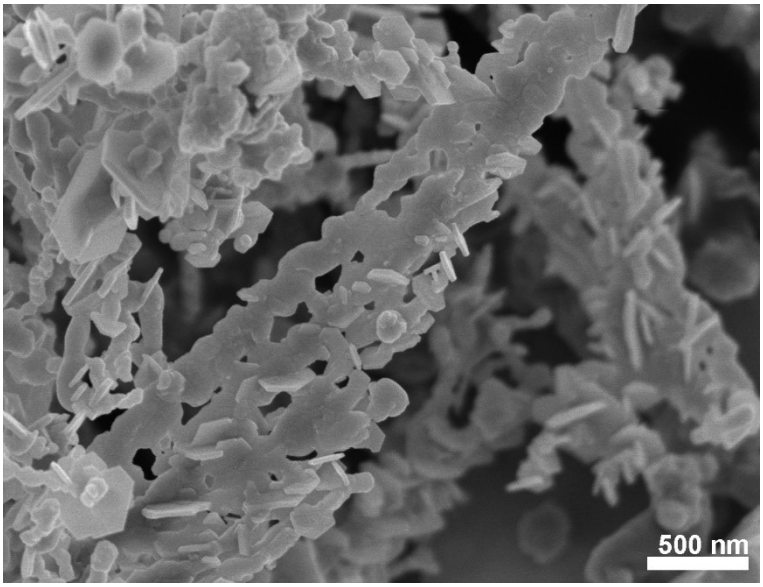

Figure S3. SEM images of Mo/Mo_2C@CoO@NC heterostructures.

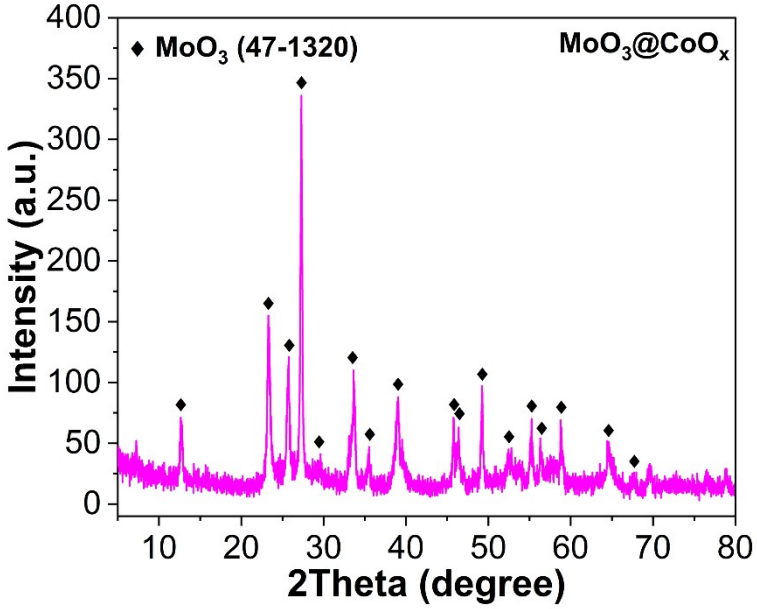

Figure S4. XRD patterns of MoO_3@CoO_x catalysts.

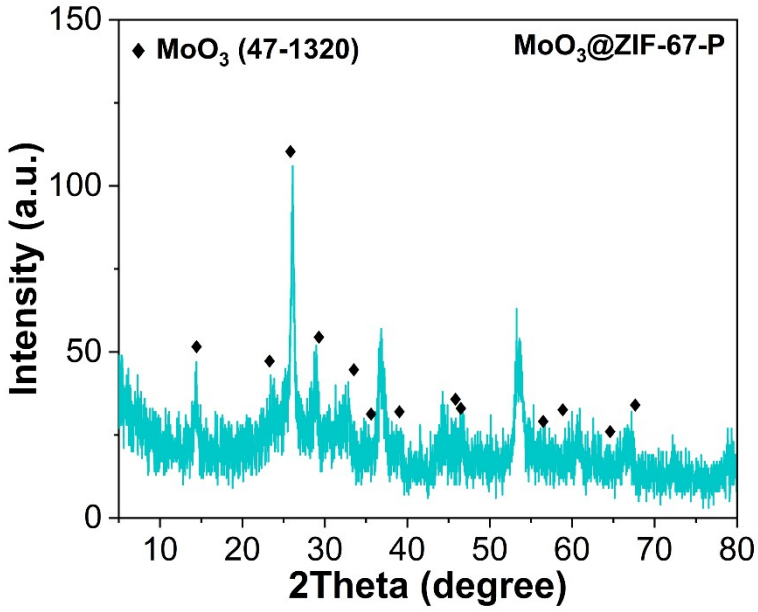

Figure S5. XRD patterns of MoO_3@ZIF-67-P catalysts.

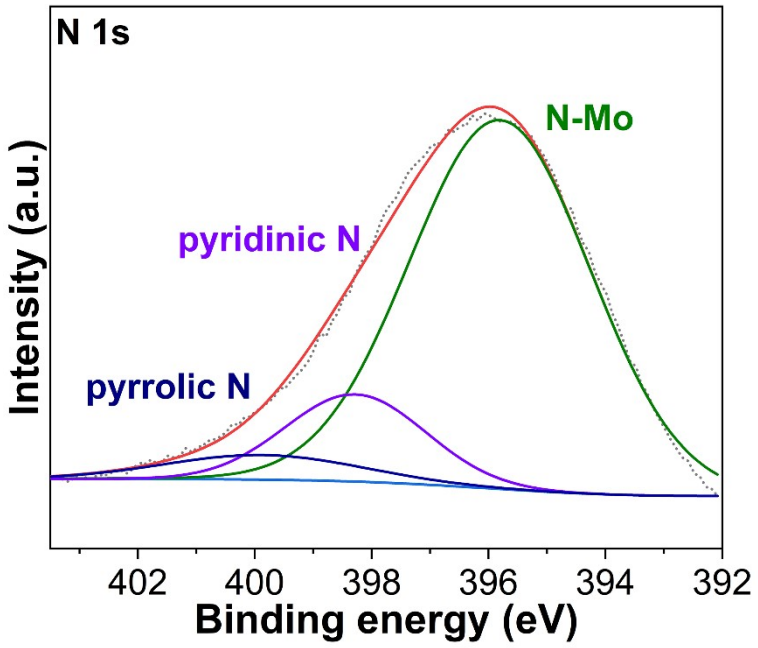

Figure S6. N 1s XPS spectra of Mo/Mo_2C@CoO@NC heterostructures.

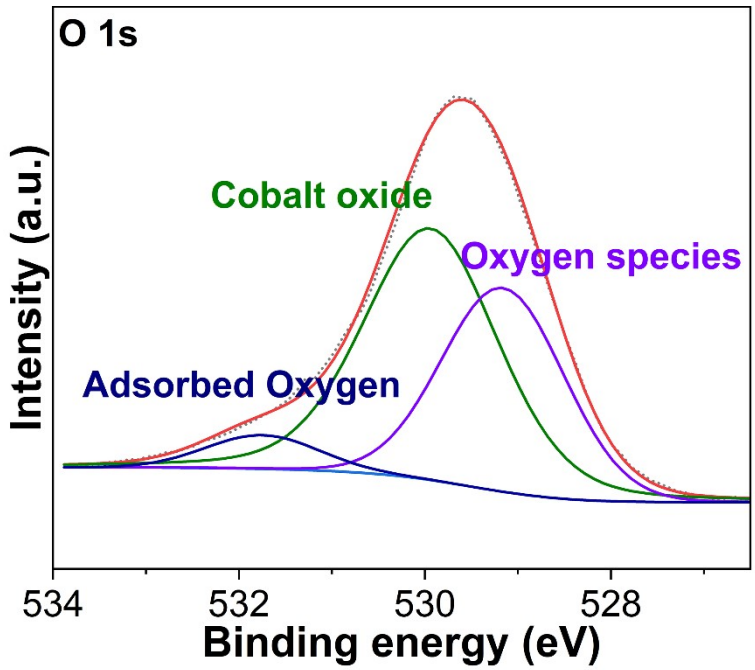

Figure S7. O 1s XPS spectra of Mo/Mo_2C@CoO@NC heterostructures.

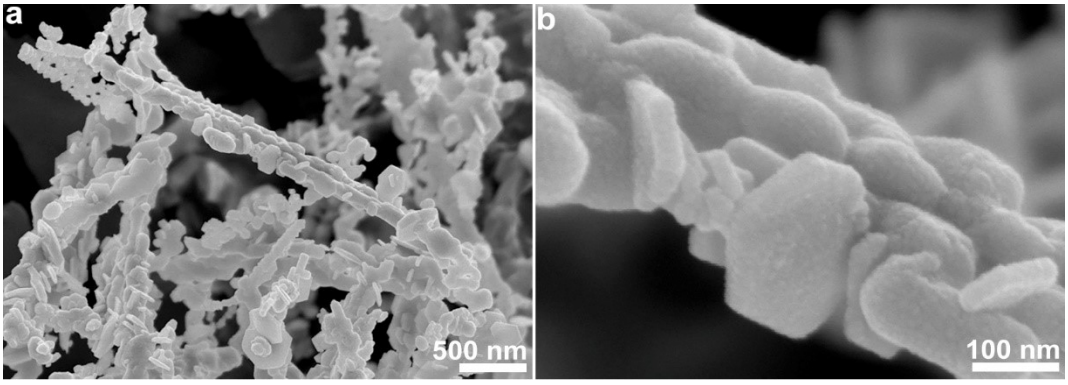

Figure S8. Low-magnification (a) and high-magnification (b) SEM images of Mo/Mo_2C@CoO@NC heterostructures.

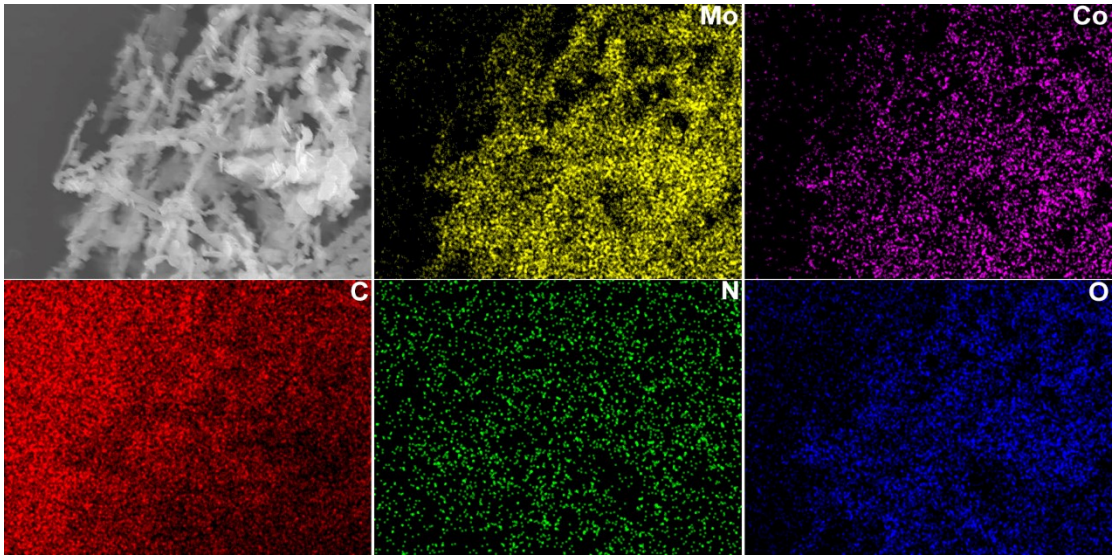

Figure S9. Elemental mapping images of Mo, Co, C, N, and O elements in $Mo/Mo_2C@CoO@NC$ heterostructures detected by SEM.

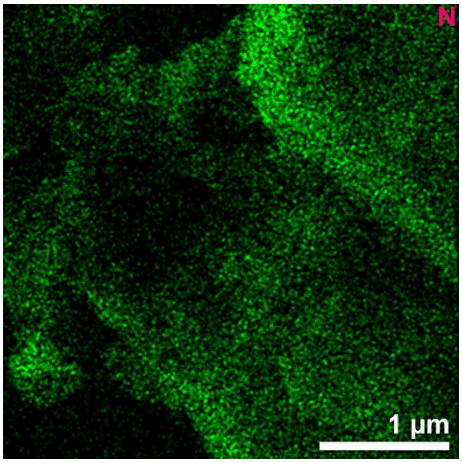

Figure S10. Elemental mapping images of N element in $Mo/Mo_2C@CoO@NC$ heterostructures detected by HAADF-STEM.

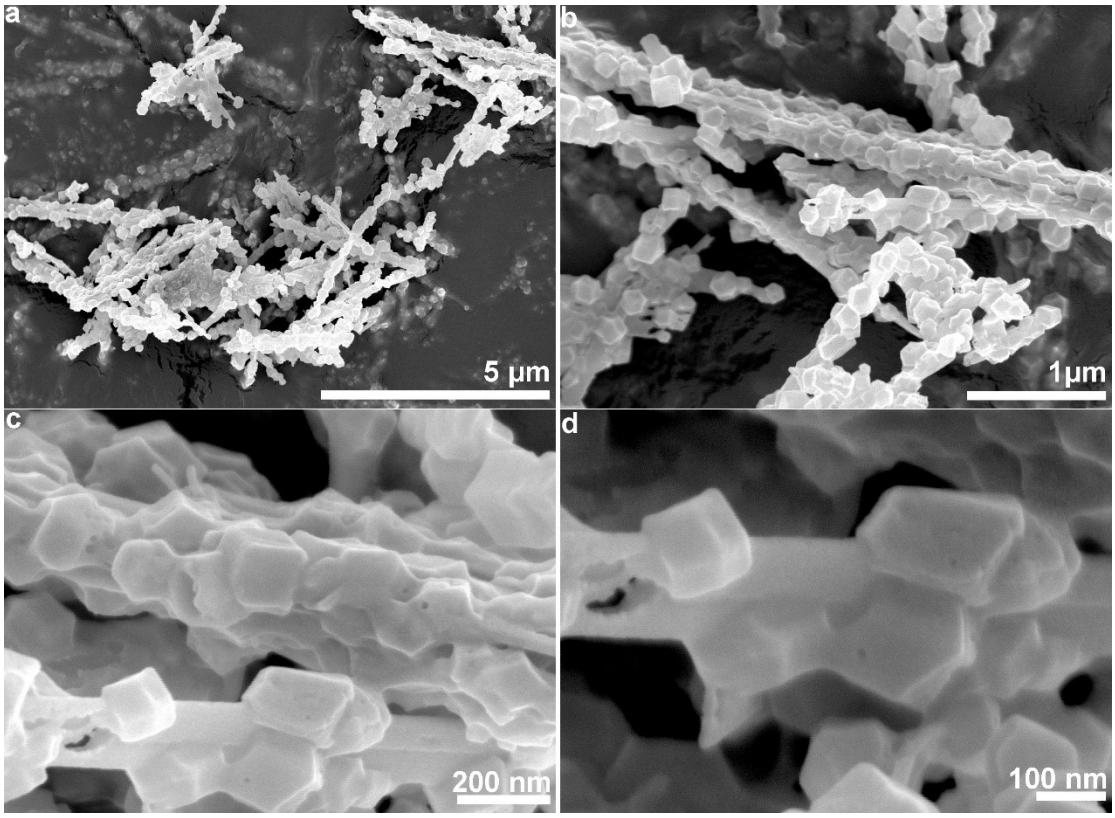

Figure S11. Low-magnification (a) and high-magnification (b-d) SEM images of MoO_3@CoO_x catalysts.

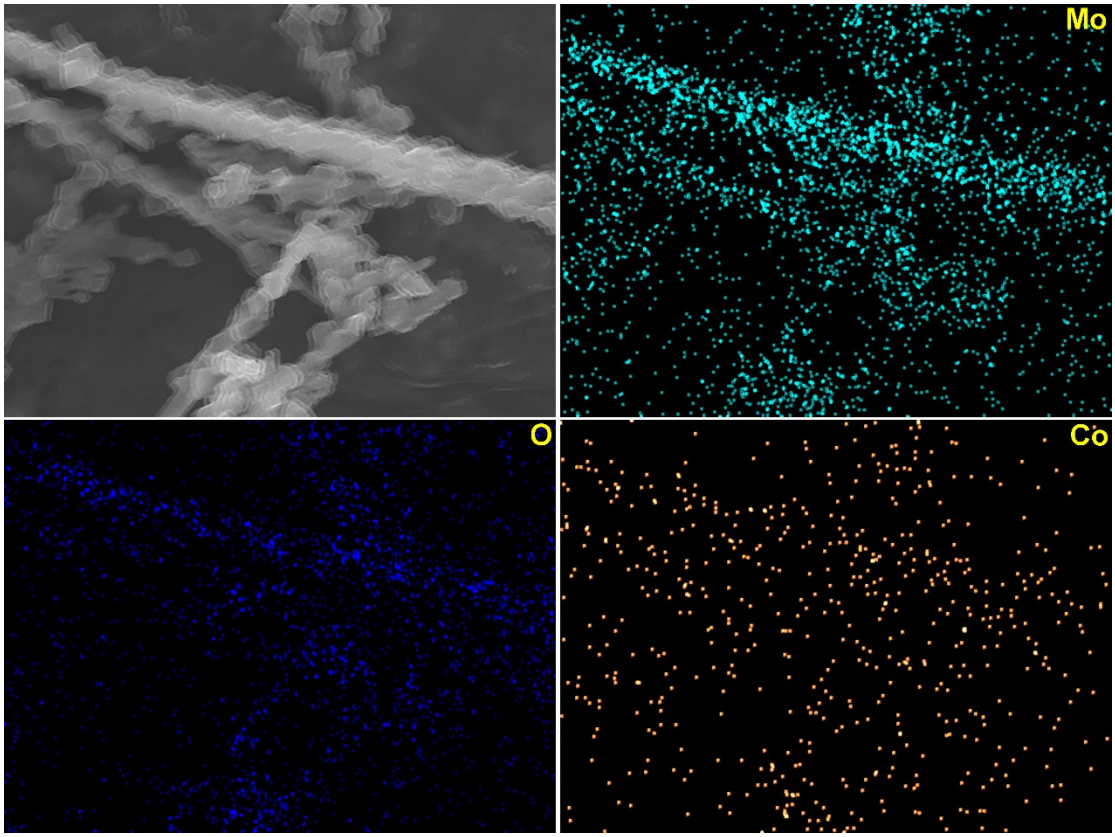

Figure S12. Elemental mapping images of Mo, O, and Co elements in MoO_3@CoO_x catalysts detected by SEM.

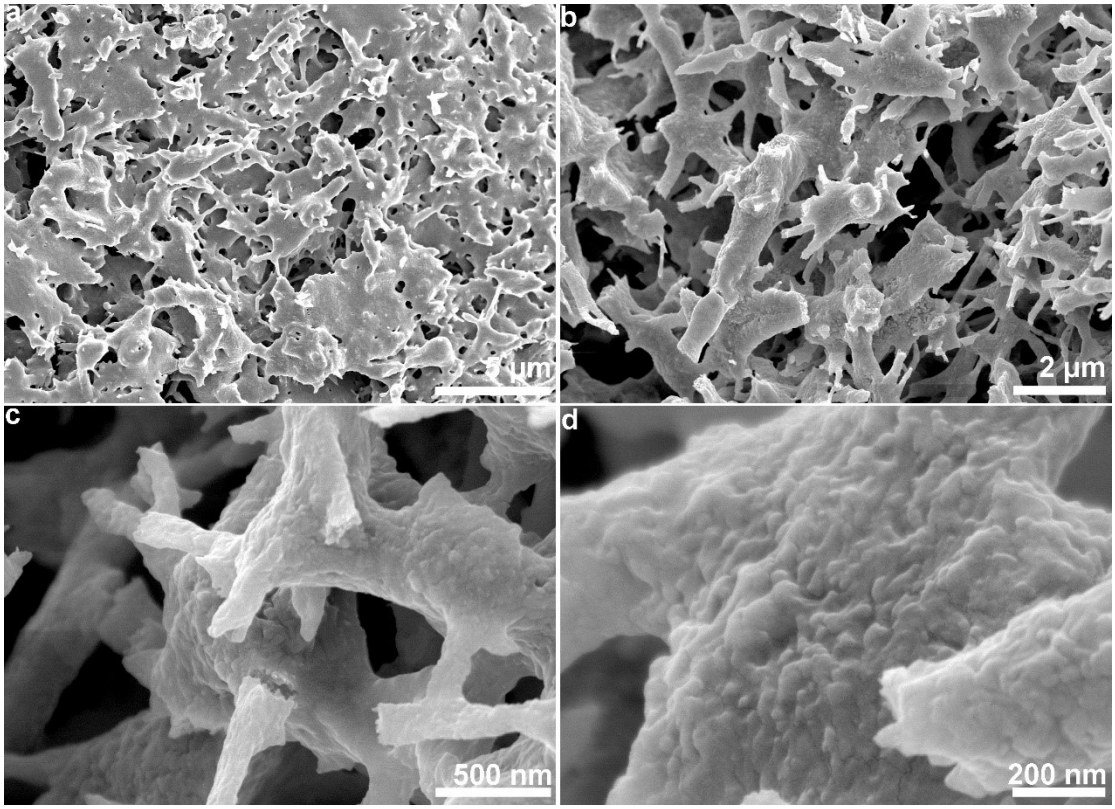

Figure S13. Low-magnification (a) and high-magnification (b-d) SEM images of MoO_3@ZIF-67-P catalysts.

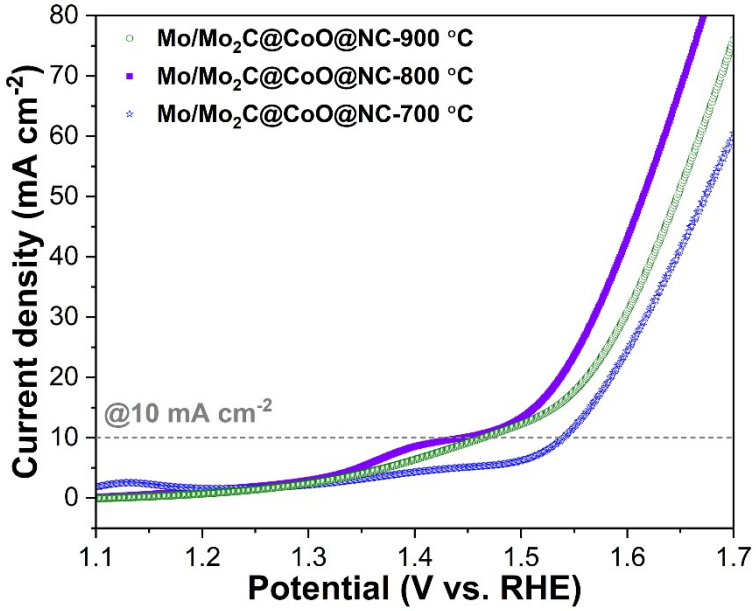

Figure S14. OER LSV polarization curves of MoO_3@ZIF-67 heterogeneous nanoribbons heat-treated at 700 °C, 800 °C, and 900 °C.

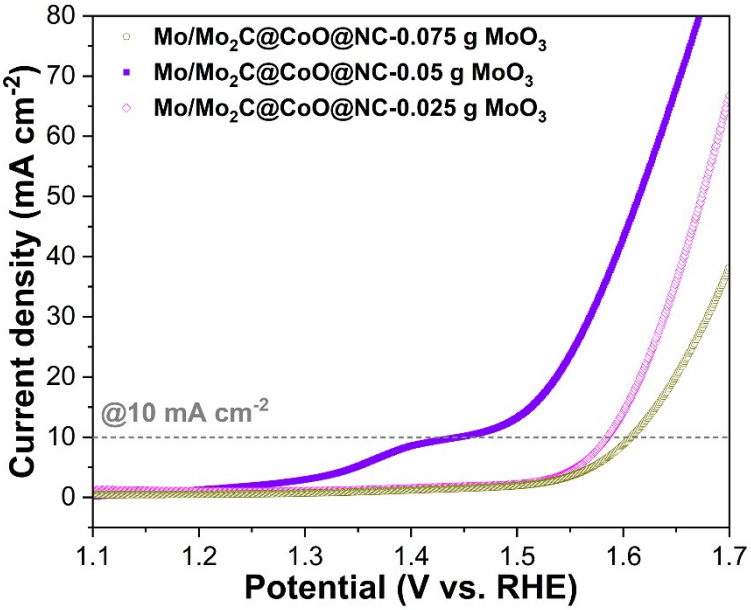

Figure S15. OER LSV polarization curves of Mo/Mo_2C@CoO@NC heterostructure with 0.025 g, 0.05 g, and 0.075 g MoO_3.

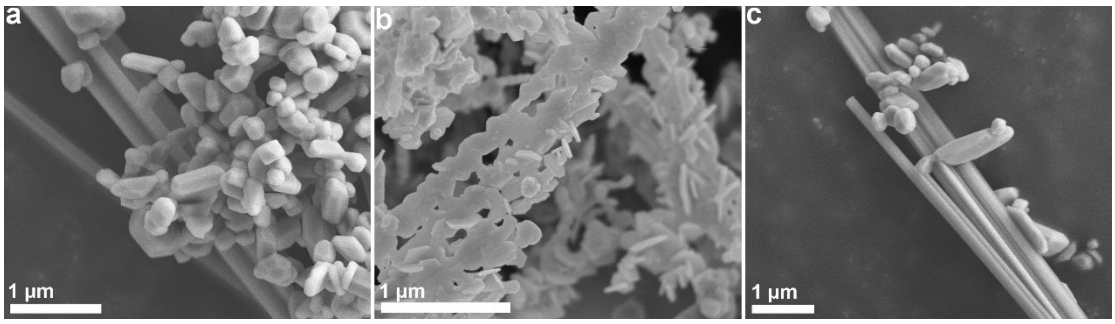

Figure S16. SEM images of Mo/Mo_2C@CoO@NC heterostructure with (a) 0.025 g, (b) 0.05 g, and (c) 0.075 g MoO_3.

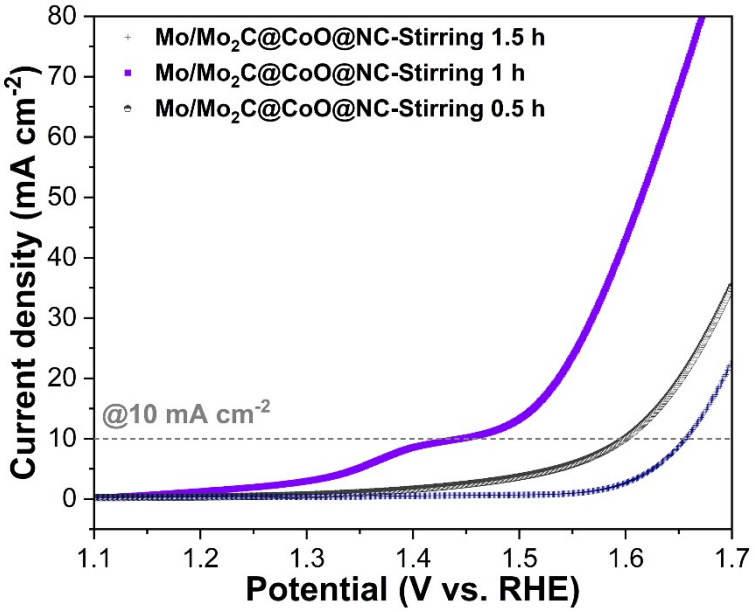

Figure S17. OER LSV polarization curves of $Mo/Mo_2C@CoO@NC$ heterostructure prepared with stirring time of 0.5 h, 1 h, and 1.5 h.

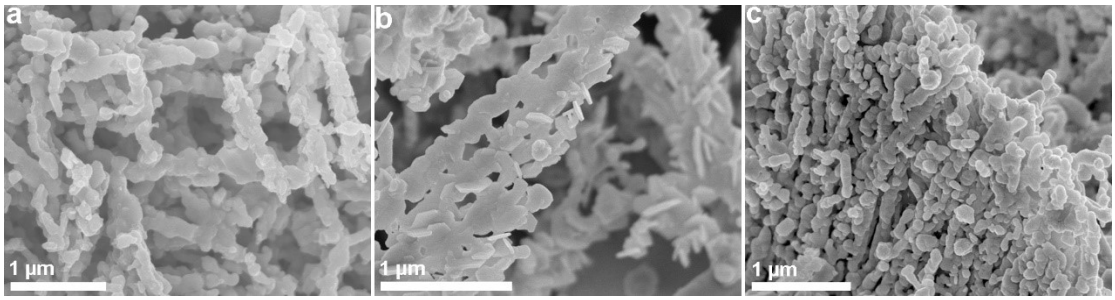

Figure S18. SEM images of $Mo/Mo_2C@CoO@NC$ heterostructure prepared with stirring time of (a) 0.5 h, (b) 1 h, and (c) 1.5 h.

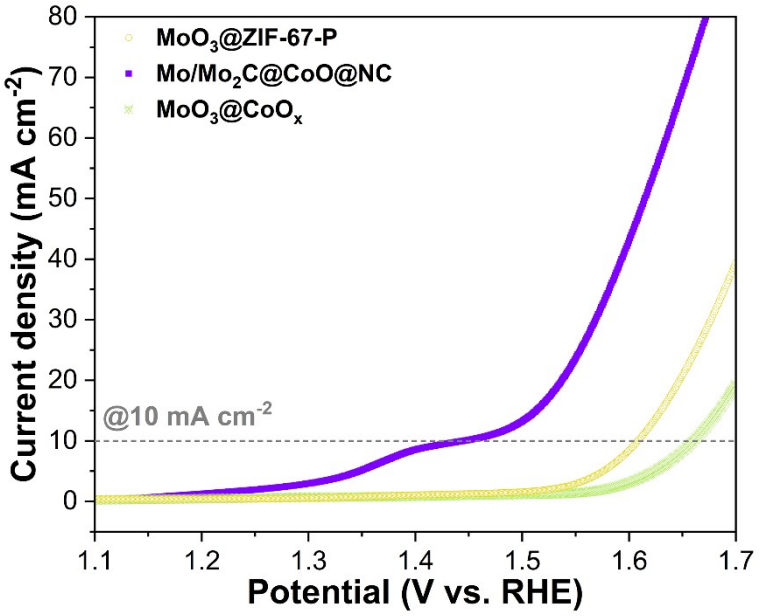

Figure S19. OER LSV polarization curves of MoO_3@ZIF-67 heterogeneous nanoribbons heat-treated in different conditions.

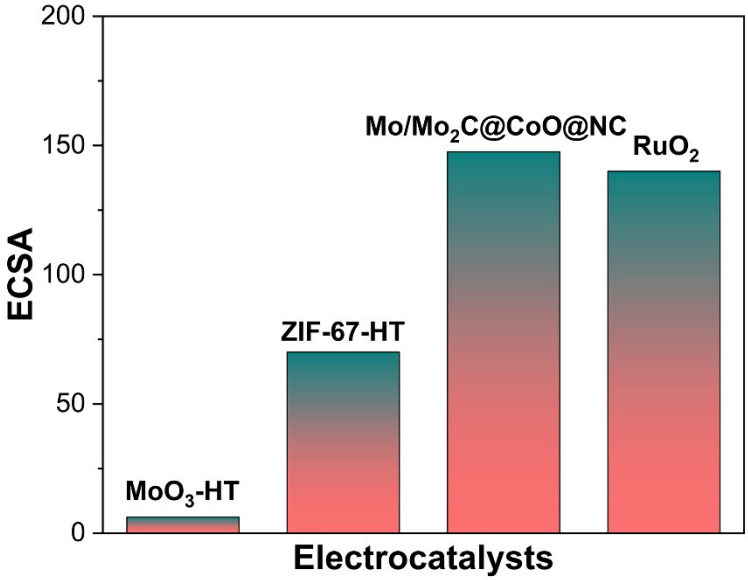

Figure S20. ECSA of MoO_3-HT, ZIF-67-HT, Mo/Mo_2C@CoO@NC, and RuO_2.

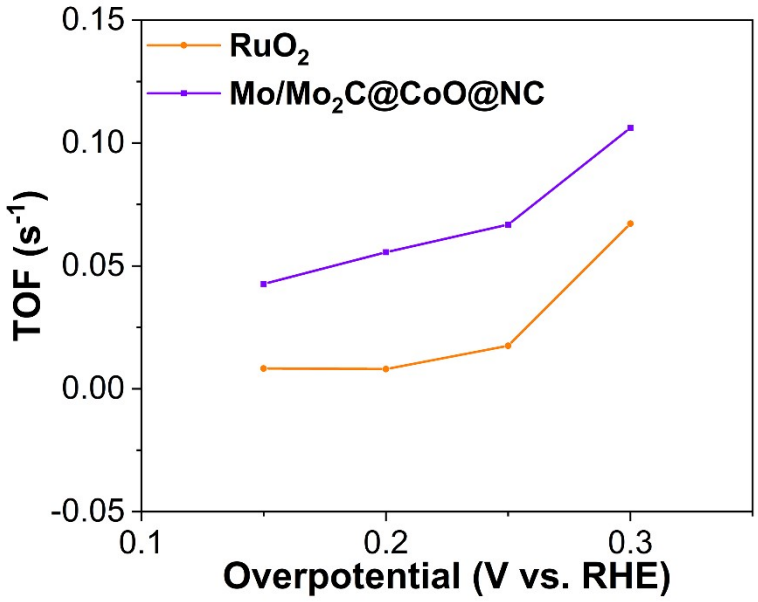

Figure S21. TOF of $Mo/Mo_2C@CoO@NC$ and RuO_2.

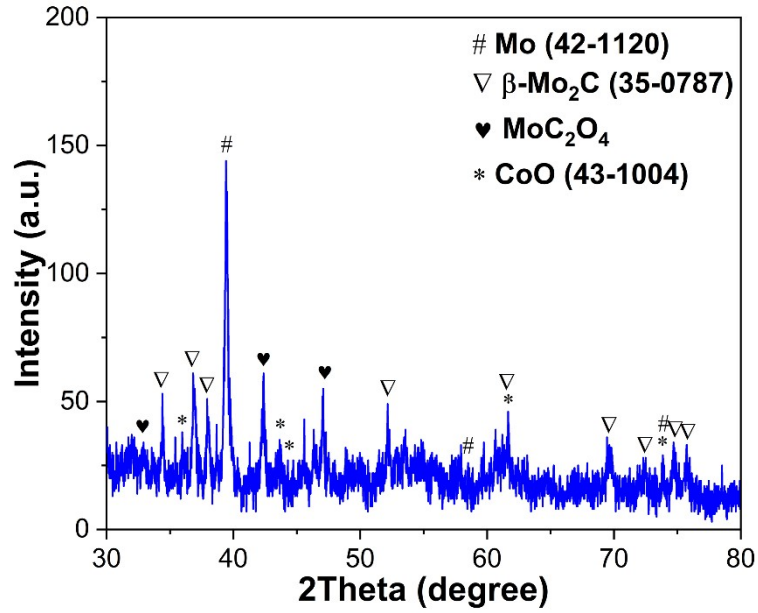

Figure S22. XRD patterns of $Mo/Mo_2C@CoO@NC$ heterostructures after chronoamperometry.

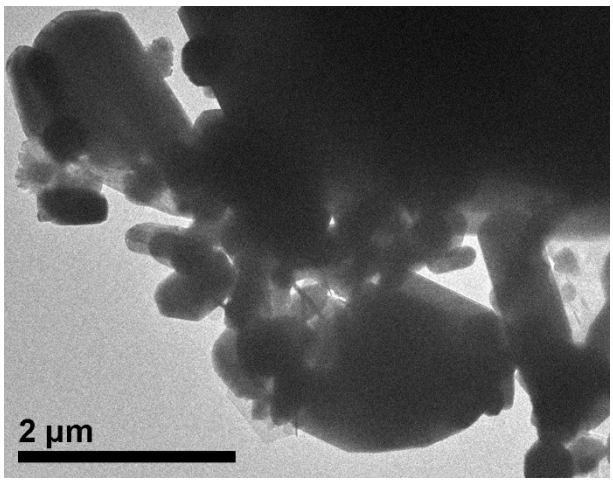

Figure S23. TEM images of $Mo/Mo_2C@CoO@NC$ heterostructures after chronoamperometry.

Table S1. Element contents in $Mo/Mo_2C@CoO@NC$ heterostructure detected by XPS technique.

Samples	Mo (At.%)	Co (At.%)	N (At.%)	C (At.%)	O (At.%)
	11.66	4.6	25.96	24.62	33.16
$Mo/Mo_2C@CoO@NC$	Mo (wt.%)	Co (wt.%)	N (wt.%)	C (wt.%)	O (wt.%)
	43.37	10.51	14.09	11.46	20.57

Table S2. Electrocatalytic performances toward OER of $Mo/Mo_2C@CoO@NC$ and recently advanced non-noble-based OER electrocatalysts.

Electrocatalysts	Loading (mg cm^{-2})	OER η (mV) @10 mA cm^{-2}	Electrolyte	Ref.
ACTP5@Co,N-800	0.30	374	0.1 M KOH	[2]
CoV_2O_6	0.23	360	1 M KOH	[3]
BP-CN-c	0.50	350	1 M KOH	[4]
MnSAC	0.10	350	0.1 M KOH	[5]
$CoNi_{40}$-MOFNs@MXene	0.20	346	1 M KOH	[6]
GNiPy350N	-	320	1 M KOH	[7]
CoFe PBA@CoP/NF	-	312	1 M KOH	[8]
Fe-Co-CN/rGO-700	0.25	308	1 M KOH	[9]
Mo_2C/Co@NC	1.00	308	1 M KOH	[10]
CoSA/N,S-HCS	1.50	306	1 M KOH	[11]
LC-CoOOH NAs/CFC	-	294	1 M KOH	[12]
P-Co_3O_4	0.30	290	1 M KOH	[13]
Vo-$MnCo_2O_4$	0.40	290	1 M KOH	[14]
$FeNi_2S_4$ NPs/CB	0.10	290	1 M KOH	[15]
FeNi-Mo_2C/C	0.07	288	1 M KOH	[16]
NiFeP/MXene	0.25	286	1 M KOH	[17]

Ni/Ni_2P@N-CNF	0.25	285	1 M KOH	[18]
P_{30}-doped Fe/NF	-	284	1 M KOH	[19]
Co/CoO@COF	0.26	278	1 M KOH	[20]
$NiCo_{2-x}Fe_xO_4$	0.50	274	1 M KOH	[21]
$Fe_{0.4}Co_{0.6}Se_2$		270	1 M KOH	[22]
Co-MOF-NK	1.00	268	1 M KOH	[23]
$Co_2P@Ti_3C_2T_x$	5.70	267	1 M KOH	[24]
NiCo LDH-TPA	2.00	267	1 M KOH	[25]
$Co(OH)_2$/NiMo CA@CC	-	267	1 M KOH	[26]
$NiFe_{0.2}$-O_xH_y	0.20	263	1 M KOH	[27]
Fe-Co-O/Co@NC-mNS/NF	-	257	1 M KOH	[28]
NiFeLDH-Bir	2.50	258	6 M KOH	[29]
NiFe-MOF/G	0.30	258	1 M KOH	[30]
NiFeLa-LDH/v-MXene	-	255	1 M KOH	[31]
FeNi-LDH-V_2C MXene	0.35	250	1 M KOH	[32]
$NiPS_{3-x}Se_x$	1.00	250	1 M KOH	[33]
Co-C@NiFe LDH	0.82	249	1 M KOH	[34]
NiFe LDH/NF-IH	-	246	1 M KOH	[35]
FeS_2@MXene	1.00	240	1 M KOH	[36]
Fe-CoP	-	237	1 M KOH	[37]
Ni_8Fe_2-MI/OH	0.26	229	1 M KOH	[38]
$(Ni_xFe_{1-x})_2P$@pc/PG	2.40	220	1 M KOH	[39]
a-LNFBPO@Ni	3.00	215	1 M KOH	[40]
Mo/Mo_2C@CoO@NC	0.20	215	1 M KOH	This work
CIF:FeNiMo-II	1.00	203	1 M KOH	[41]
$Ni_{0.9}Fe_{0.1}$-MOF	0.20	198	1 M KOH	[42]

References

[1] Wang J. J.; Zeng, H. C. Hybrid OER electrocatalyst combining mesoporous hollow spheres of N, P-doped carbon with ultrafine Co_2NiO_x. ACS *Appl. Mater. Interfaces* **2020**, *12*, 50324−50332.

[2] Zhang, J. T.; Zhang, T.; Ma, J.; Wang, Z.; Liu, J. H.; Gong, X. Z. ORR and OER of Co-N codoped carbon-based electrocatalysts enhanced by boundary layer oxygen molecules transfer. *Carbon* **2021**, *172*, 556–568.

[3] Mondal, A.; Ganguli, S.; Inta, H. R.; Mahalingam, V. Influence of Vanadate Structure on Electrochemical Surface Reconstruction and OER Performance of CoV_2O_6 and $Co_3V_2O_8$. *ACS Appl. Energy Mater*. **2021**, *4, 6*, 5381–5387.

[4] Wang, X.; Raghupathy, R. K. M.; Querebillo, C. J.; Liao, Z. Q.; Li, D. Q.; Lin, K.; Hantusch, M.; Sofer, Z.; Li, B. H.; Zschech, Z.; Weidinger, I. M.; Kühne, T. D.; Mirhosseini, H.; Yu, M. H.; Feng, X. L. Interfacial Covalent Bonds Regulated Electron-Deficient 2D Black Phosphorus for Electrocatalytic Oxygen Reactions. *Adv. Mater*. **2021**, *33*, 2008752.

[5] Shang, H. S.; Sun, W. M.; Sui, R.; Pei, J. J.; Zheng, L. R.; Dong, J. C.; Jiang, Z. L.; Zhou, D. N.; Zhuang, Z. B.; Chen, W. X.; Zhang, J. T.; Wang, D. S.; Li, Y. D. Engineering Isolated Mn-N_2C_2 Atomic Interface Sites for Efficient Bifunctional Oxygen Reduction and Evolution Reaction. *Nano Lett*. **2020**, *20*, 5443–5450.

[6] Du, C.-F.; Song, Q. Q.; Liang, Q. H.; Zhao, X. Y.; Wang, J. J.; Zhi, R. C.; Wang, Y. X.; Yu, H. The Passive Effect of MXene on Electrocatalysis: A Case of $Ti_3C_2T_x$/CoNi-MOF nanosheets for Oxygen Evolution Reaction. *ChenNanoMat* **2021**,

7, 539–544.

[7] Souza, A. S.; Bezerra, L. S.; Cardoso, E. S. F.; Fortunato, G. V.; Maia, G. Nickel pyrophosphate combined with graphene nanoribbon used as efficient catalyst for OER. *J. Mater. Chem. A* **2021**, *9*, 11255–11267.

[8] Quan, L.; Li, S. H.; Zhao, Z. P.; Liu, J. Q.;Ran, Y.; Cui, J. Y.; Lin, W.; Yu, X. L.; Wang, L.; Zhang, Y. H.; Ye, J. H. Hierarchically Assembling CoFe Prussian Blue Analogue Nanocubes on CoP Nanosheets as Highly Efficient Electrocatalysts for Overall Water Splitting. *Small Methods* **2021**, 2100125.

[9] Fang, W. H.; Wang, J.; Hu, Y.; Cui, X. Q.; Zhu, R. F.; Zhang, Y. H.; Yue, C. C.; Dang, J. Q.; Cui, W.; Zhao, H.; Li, Z. X. Metal-Organic Framework Derived Fe-Co-CN/Reduced Graphene Oxide for Efficient HER and OER. *Electrochim. Acta* **2021**, *365*, 137384.

[10] Gu, T. T.; Sa, R. J.; Zhang, L. J.; Li, D. S.; Wang, R. H. Engineering interfacial coupling between Mo_2C nanosheets and Co@NC polyhedron for boosting electrocatalytic water splitting and zinc-air batteries. *Appl. Catal. B* **2021**, *296*, 120360.

[11] Zhang, Z. Y.; Zhao, X. X.; Xi, S. B.; Zhang, L. L.; Chen, Z. X.; Zeng, Z. P.; Huang, M.; Yang, H. B.; Liu, B.; Pennycook, S. J.; Chen, P. Atomically Dispersed Cobalt Trifunctional Electrocatalysts with Tailored Coordination Environment for Flexible Rechargeable Zn-Air Battery and Self-Driven Water Splitting. *Adv. Energy Mater*. **2020**, *10*, 2002896.

[12] Ye, S. H.; Wang, J. P.; Hu, J.; Chen, Z. D.; Zheng, L. R.; Fu, Y. H.; Lei, Y. Q.;

Ren, X. Z.; He, C. X.; Zhang, Q. L.; Liu, J. H. Electrochemical Construction of Low-Crystalline CoOOH Nanosheets with Short-Range Ordered Grains to Improve Oxygen Evolution Activity. *ACS Catal*. 2021, 11, 6104–6112.

[13] Lu, Y.; Li, C. J.; Zhang, Y.; Cao, X.; Xie, G.; Wang, M. L.; Peng, D. D.; Huang, K.; Zhang, B. W; Wang, T.; Wu, J. S.; Huang, Y. Z. Engineering of cation and anion vacancies in Co_3O_4 thin nanosheets by laser irradiation for more advancement of oxygen evolution reaction. *Nano Energy* **2021**, *83*, 105800.

[14] Zeng, K.; Li, W.; Zhou, Y.; Sun, Z. H.; Lu, C. Y.; Yan, J.; Choi, J. H.; Yang, R. Z. Multilayer Hollow $MnCo_2O_4$ Microsphere with Oxygen Vacancies as Efficient Electrocatalyst for Oxygen Evolution Reaction. *Chem. Eng. J*. **2021**, *421*, 127831.

[15] Jiang, J.; Zhang, Y. J.; Zhu, X. J.; Lu, S.; Long, L. L.; Chen, J. J. Nanostructured metallic $FeNi_2S_4$ with reconstruction to generate FeNi-based oxide as a highly-efficient oxygen evolution electrocatalyst. *Nano Energy* **2021**, *81*, 105619.

[16] Wang, M.; Wang, Y. Q.; Mao, S. S.; Shen, S. H. Transition-metal alloy electrocatalysts with active sites modulated by metal-carbide heterophases for efficient oxygen evolution. *Nano Energy* **2021**, *88*, 106216.

[17] Chen, J. X.; Long, Q. W.; Xiao, K.; Ouyang, T.; Li, N.; Ye, S. Y.; Liu, Z.-Q. Vertically-interlaced NiFeP/MXene electrocatalyst with tunable electronic structure for high-efficiency oxygen evolution reaction. *Sci. Bull.* **2021**, *66*, 1063–1072.

[18] Li, X. G.; Zhou, J. H.; Liu, C.; Xu, L.; Lu, C. L.; Yang, J.; Pang, H.; Hou, W. H. Encapsulation of Janus-structured Ni/Ni_2P nanoparticles within hierarchical wrinkled N-doped carbon nanofibers: Interface engineering induces high-efficiency water

oxidation. *Appl. Catal. B* **2021**, *298*, 120578.

[19] Ju, Y.; Feng, S. Y.; Wang, X. B.; Li, M.; Wang, L.; Xu, R. D.; Wang, J. L. Facile Preparation of a Porous Nanosheet PX-Doped Fe BiFunctional Catalyst with Excellent OER and HER Electrocatalytic Activity. *ChemistrySelect* **2021**, *6*, 4979–4990.

[20] Ye, X. Q.; Fan, J. C.; Min, Y. L.; Shi, P. H.; Xu, Q. J. Synergistic Effect of Co/CoO Nanoparticles on Imine-based Covalent Organic Framework for Enhanced OER Performance. *Nanoscale* **2021**, 13, 14854–14865.

[21] Huang, Y.; Zhang, S. L.; Lu, X. F.; Wu, Z. P.; Luan, D. Y.; Lou, X. W. Trimetallic Spinel $NiCo_{2-x}Fe_xO_4$ Nanoboxes for Highly Efficient Electrocatalytic Oxygen Evolution. *Angew. Chem. Int. Ed*. **2021**, *60*, 11841–11846.

[22] Zhang, J. Y.; Yan, Y.; Mei, B. B.; Qi, R. J.; He, T.; Wang, Z. T.; Fang, W. S.; Zaman, S.; Su, Y. Q.; Ding, S. J.; Xia, B. Y. Local spin-state tuning of cobalt-iron selenide nanoframes for the boosted oxygen evolution. *Energy Environ. Sci*. **2021**, *14*, 365–373.

[23] Liu, M.; Kong, L. J.; Wang, X. M.; He, J.; Zhang, J. J.; Zhu, J.; Bu, X. H. Deciphering of advantageous electrocatalytic water oxidation behavior of metal-organic framework in alkaline media. *Nano Res*. **2021**, 1–9.

[24] Lv, Z. P.; Ma, W. S.; Dang, J.; Wang, M.; Jian, K. L.; Liu, D.; Huang, D. J. Induction of Co_2P Growth on a MXene ($Ti_3C_2T_x$)-Modified Self-Supporting Electrode for Efficient Overall Water Splitting. *J. Phys. Chem. Lett.* **2021**, *12*, 4841–4848.

[25] Liu, W. X.; Zheng, D.; Deng, T. Q.; Chen, Q. L.; Zhu, C. Z.; Pei, C. J.; Li, H.; Wu, F. F.; Shi, W. H.; Yang, S. W.; Zhu, Y. H.; Cao, X. H. Boosting Electrocatalytic

Activity of 3d-Block Metal (Hydro)oxides by Ligand-Induced Conversion. *Angew. Chem. Int. Ed.* 2021, 60, 10614–10619.

[26] Zhang, Q.; Xiao, W.; Guo, W. H.; Yang, Y. X.; Lei, J. L.; Luo, H. Q.; Li, N. B. Macroporous Array Induced Multiscale Modulation at the Surface/Interface of $Co(OH)_2$/NiMo Self-Supporting Electrode for Effective Overall Water Splitting. *Adv. Funct. Mater*. **2021**, 2102117.

[27] Kuang, Z. C.; Liu, S.; Li, X. N.; Wang, M.; Ren, X. Y.; Ding, J.; Ge, R.; Zhou, W. H.; Rykov, A. L.; Sougrati, M. T.; Lippens, P. E.; Huang, Y. Q.; Wang, J. H. Topotactically constructed nickel-iron (oxy)hydroxide with abundant in-situ produced high-valent iron species for efficient water oxidation. *J. Energy Chem*. 2021, 57, 212–218.

[28] Singh, T. I.; Rajeshkhanna, G.; Pan, U. N.; Kshetri, T.; Lin, H.; Kim, N. H.; Lee, J. H. Alkaline Water Splitting Enhancement by MOF-Derived Fe-Co-Oxide/Co@NC-mNS Heterostructure: Boosting OER and HER through Defect Engineering and In Situ Oxidation. *Small* **2021**, *17*, 2101312.

[29] Chen, Z. W.; Ju, M.; Sun, M. Z.; Jin, L.; Cai, R. M.; Wang, Z.; Dong, L.; Peng, L. M.; Long, X.; Huang, B. L.; Yang, S. H. TM LDH Meets Birnessite: A 2D-2D Hybrid Catalyst with Long-Term Stability for Water Oxidation at Industrial Operating Conditions. *Angew. Chem. Int. Ed*. **2021**, *60*, 9699–9705.

[30] Wang, Y.; Liu, B. R.; Shen, X. J.; Arandiyan, H.; Zhao, T. W.; Li, Y. B.; Garbrecht, M.; Su, Z.; Han, L.; Tricoli, A.; Zhao, C. Oxygen Evolution Reaction: Engineering the Activity and Stability of MOF-Nanocomposites for Efficient Water Oxidation. *Adv.*

Energy Mater. **2021**, *11*, 2003759.

[31] Yu, M. Z.; Zheng, J. Q.; Guo, M. La-doped NiFe-LDH coupled with hierarchical vertically aligned MXene frameworks for efficient overall water splitting. *J. Energy Chem.* **2022**, *70*, 472–479.

[32] Chen, Y. F.; Yao, H. L.; Kong, F. T.; Tian, H.; Meng, G.; Wang, S. Z.; Mao, X. P.; Cui, X. Z.; Hou, X. M.; Shi, J. L. MXene-induced electronic optimization of metal-organic framework-derived CoFe LDH nanosheet arrays for efficient oxygen evolution. *Appl. Catal. B* **2021**, *297*, 120474.

[33] Song, J. N.; Qiu, S. Y.; Hu, F.; Ding, Y. H.; Han, S. L.; Li, L. L.; Chen, H. Y.; Han, X. P.; Sun, C. H.; Peng, S. J. Sub-2 nm Thiophosphate Nanosheets with Heteroatom Doping for Enhanced Oxygen Electrocatalysis. *Adv. Funct. Mater*. **2021**, *31*, 2100618.

[34] Li, W. M.; Chen, S. H.; Zhong, M. X.; Wang, C.; Lu, X. F. Synergistic coupling of NiFe layered double hydroxides with Co-C nanofibers for high-efficiency oxygen evolution reaction. *Chem. Eng. J*. **2021**, *415*, 128879.

[35] Xiong, G. W.; Chen, Y. K.; Zhou, Z. Q.; Liu, F.; Liu, X. Y.; Yang, L.J.; Liu, Q. L.; Sang, Y. H.; Liu, H.; Zhang, X. L.; Jia, J.; Zhou, W. J. Rapid Synthesis of Various Electrocatalysts on Ni Foam Using a Universal and Facile Induction Heating Method for Efficient Water Splitting. *Adv. Funct. Mater*. **2021**, *31*, 2009580.

[36] Xie, Y. Y.; Yu, H. Z.; Deng, L. M.; Amin, R. S.; Yu, D. S.; Fetohi, A. E.; Maximov, M. Yu.; Li, L. L.; El-Khatib, K. M.; Peng, S. J. Anchoring stable FeS_2 nanoparticles on MXene nanosheets *via* interface engineering for efficient water splitting. *Inorg. Chem.*

Front. **2022**, *9*, 662–669.

[37] Yu, X. W.; Zhao, J.; Johnsson, M. Interfacial Engineering of Nickel Hydroxide on Cobalt Phosphide for Alkaline Water Electrocatalysis. *Adv. Funct. Mater*. **2021**, *31*, 2101578.

[38] Huang, W. Z.; Chen, C. X.; Ling, Z. H.; Li, J. T.; Qu, L. B.; Zhu, J. X.; Yang, W.; Wang, M. M.; Owusu, K. A.; Qin, L.; Zhou, L.; Mai, L. Q. Ni/Fe based bimetallic coordination complexes with rich active sites for efficient oxygen evolution reaction. *Chem. Eng. J*. **2021**, *405*, 126959.

[39] Wang, L.; Fan, J. Y.; Liu, Y.; Chen, M. Y.; Lin, Y.; Bi, H. C.; Liu, B. X.; Shi, N. E.; Xu, D. D.; Bao, J. C.; Han, M. Phase-Modulation of Iron/Nickel Phosphides Nanocrystals "Armored" with Porous P-Doped Carbon and Anchored on P-Doped Graphene Nanohybrids for Enhanced Overall Water Splitting. *Adv. Funct. Mater*. **2021**, *31*, 2010912.

[40] Kwon, J.; Han, H.; Jo, S.; Choi, S.; Chung, K. Y.; Ali, G.; Park, K.; Paik, U.; Song, T. Amorphous Nickel-Iron Borophosphate for a Robust and Efficient Oxygen Evolution Reaction. *Adv. Energy Mater*. **2021**, *11*, 2100624.

[41] Choi, W. H.; Kim, K. H.; Lee, H.; Choi, J.W.; Park, D. G.; Kim, G. H.; Choi, K. M.; Kang, J. K. Metal-Organic Fragments with Adhesive Excipient and Their Utilization to Stabilize Multimetallic Electrocatalysts for High Activity and Robust Durability in Oxygen Evolution Reaction. *Adv. Sci*. **2021**, *8*, 2100044.

[42] Zhao, S. L.; Tan, C. H.; He, C. T.; An, P. F.; Xie, F.; Jiang, S.; Wu, K. H.; Zhang, B. W.; Li, H. J.; Zhang, J.; Chen, Y.; Liu, S. Q.; Dong, J. C.; Tang, Z. Y. Structural

transformation of highly active metal-organic framework electrocatalysts during the oxygen evolution reaction. *Nat. Energy* **2020**, *5*, 881–890.